International Conference on Space Optics—ICSO 2022

Dubrovnik, Croatia

3–7 October 2022

Edited by Kyriaki Minoglou, Nikos Karafolas, and Bruno Cugny,

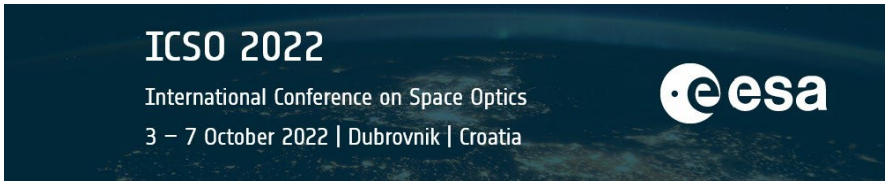

An account of the Euclid payload module test results

International Conference on Space Optics — ICSO 2022, edited by Kyriaki Minoglou, Nikos Karafolas, Bruno Cugny, Proc. of SPIE Vol. 12777, 127776H · © 2023 ESA and CNES · 0277-786X · doi: 10.1117/12.2691130

An account of the Euclid payload module test results

Luis Gaspar Venancio*[a], René Laureijs[a], Giuseppe Racca[a], Elena Maiorano[a], Alex Short[a], Tobias Boenke[a], Paolo Strada[a], Magdalena Szafraniec[a], Roland Vavrek[a]
[a]European Space Agency, ESTEC, Keplerlaan 1, 2201 AZ Noordwijk, The Netherlands

ABSTRACT

The Euclid mission, the spacecraft being the essential space element, has been developed to undertake the challenges of investigate the dark energy and dark matter distribution in the Universe. As the launch date is approaching, the telescope and the integrated payload, encompassing the telescope and with the two science instruments attached behind it, have been successfully tested. The telescope alone was tested under ambient conditions, and the integrated payload was tested in vacuum at operational temperature. The extensive test campaign at telescope level confirmed that its optical performance were better than the required levels. The thermal-vacuum test campaign demonstrated the excellent stability of the optical performance of the entire payload module. In addition, other performances of the integrated payload were tested to gather information on the behavior of the payload which will be used for the preparation of the calibrations in-flight.

Keywords: Euclid, tests, payload, performance, experiments

1. INTRODUCTION

Euclid is a high-precision survey mission designed to map the distribution of dark matter and investigate the nature of the dark energy in the Universe. The mission will implement two probes: Weak Lensing (WL) and Galaxy Clustering (GC) that is used to investigate Baryonic Acoustic Oscillations (BAO). These probes require a high image quality, near-infrared spectroscopic and optical imaging capabilities and very high system stability to minimize systematic effects. The probes require the imaging of two billions of galaxies over a sky area covering 15000 deg2 and the spectrometric redshift measurement of tens of millions of galaxies. Such mission constraints[1] are directly translated in the design and manufacturing of the space segment of the mission[2].

The Euclid's space segments consists of a single spacecraft including two main modules: the service module (SVM) and the Payload Module (PLM), see both represented in Figure 1. The present paper focuses on the PLM briefly described hereafter, its detailed design and architecture of the PLM being described elsewhere[3]. The PLM comprises a 1.2-m class Korsch-type telescope directing the incoming light towards two separated instruments: the VISible imager(VIS)[4] and the Near-Infrared Spectrometer & Photometer(NISP)[5][6] , the light is spectrally split between instruments by a dichroic plate. The telescope structure and its mirrors are made out of Silicon Carbide (SiC) to maximize the stability of the optical performance against thermal perturbations of the image quality delivered to the instruments. The telescope has a refocusing and tip/tilt capability implemented with a mechanism on the secondary mirror M2 to compensate for any drift in the image quality during the mission.

While the theoretical performances of the payload were extensively computed and simulated[7], the actual performances after integration and alignment remained to be determined and compared to the predictions. The validation and qualification plan of the payload, performances wise, comprises two sequential steps: 1) determination of the optical performance of the telescope alone is first determined in ambient conditions after the final alignment which includes the search for the best focus with M2; 2) verification in thermo-vacuum conditions, after integration of the instruments with the telescope, of the stability of the alignment and testing of the optical performances. The tests at ambient were performed in the Airbus Defense & Space premises in Toulouse-France. The thermal vacuum tests were performed in the Focal 5 chamber of the Centre Spatial de Liege (CSL) in Belgium.

The first part of this paper is dedicated to the ambient tests while the second part reports on the results of the thermal vacuum test campaign. In each section, the goal of the test and the equipment will be described first. The results are then reported.

* luis.miguel.gaspar.venancio@esa.int; phone +31 (0) 71 565 8054; www.esa.int

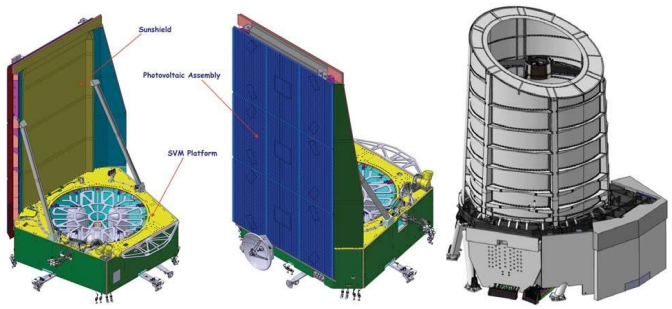

Figure 1. Euclid spacecraft overview. From left to right: front view of the SM; back view of the SVM; overview of the integrated PLM. *Courtesy of Airbus Defense&Space and Thales Alenia Space-Italy.*

2. TEST IN AMBIENT CONDITIONS

After alignment of the telescope the following properties were verified: wavefront error (WFE) of the telescope across the field of view with gravity compensated, the primary mirror quilting, the straylight baffling and the position of the exit pupil of the telescope. The tests required specific equipment which will be described here as far as possible.

2.1 WFE measurements

The WFE whas been measured in double pass using a flat mirror placed in front of the telescope entrance pupil. The light-source and a Shack-Hartman WFE sensor were placed in the focal plane of the telescope. The WFE was derived for two opposite orientations wrt gravity of the telescope over 17 field points across the field of view for two opposite telescope orientations with respect to gravity; the field points are depicted in Figure 2. These two measurements were then used to derive the WFE corrected for the effect of gravity.
Overall, the derived WFE at 0G is found to be lower than 45nm RMS over the field of view, leaving sufficient some margins wrt with respect to the specification of 60 nm RMS for the contributors linked to cool-down. Such contributors are the mirrors displacements and deformation under thermo-mechanical loads.

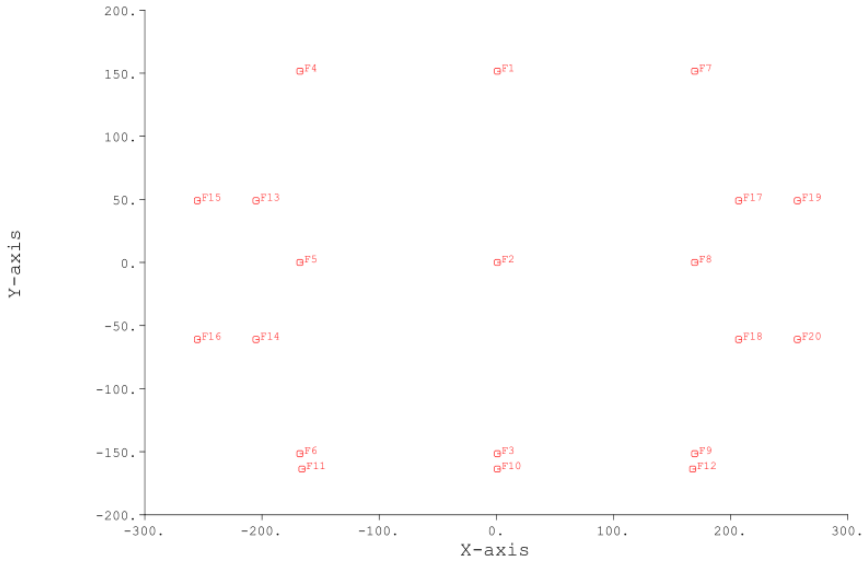

Figure 2. Field points used for the WFE measurements described in the telescope focal plane. The fields F10 to F12 were not considered during the test. Units are in millimeters.

2.2 Pupil centration

The knowledge on the location of the telescope exit pupil is necessary for the alignment of the NISP instrument behind the telescope. For such test, the Shack-Hartmann was removed and a camera was placed such to capture the image of the exit pupil when the telescope is illuminated in double-pass. The position of the exit pupil relative to the edges of the dichroic mirror were derived from the images and compared to the specification. An image of the exit pupil is presented in Figure 3. It shows the M2 obscuration and the spider arms. The edges of the dichroic are in white surrounding the exit pupil. The ghost image of the pupil is due to the camera.

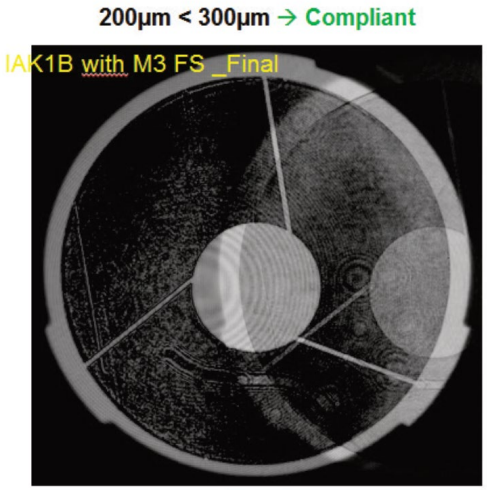

Figure 3. Image of the telescope's exit pupil for the field point F2. *Courtesy of Airbus Defense&Space.*

The alignment of the exit pupil is as specified, thus confirming that the shimming of the mirrors and alignment were successful.

2.3 Straylight

The telescope straylight is defined as the Normalised Detector Irradiance or NDI[8] The expected straylight performance[7] was specified of course for the end of life (EoL) contamination. e Immediately after alignment, the straylight performance must be better than EoL because the mirrors are still low on particulate and molecular contamination. The NDI template for the test was thus derived using the level of particulate contamination measured at the time of the test. Some part of the NDI is not driven by particulate contamination, this is why the test template in Figure 4 has 2 discontinuities at about 4 and 30 degrees. This template was used to assess the measured straylight performance.

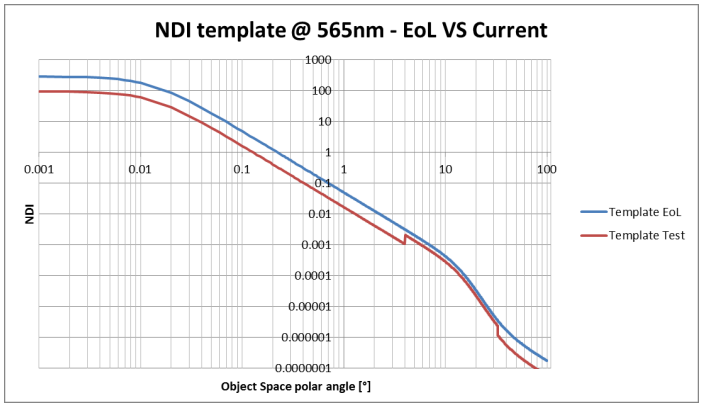

Figure 4. NDI template for the test at ambient (red) is derived from the specification end of life (blue). *Courtesy of Airbus Defense&Space.*

For the measurements, a specific equipment was developed for the straylight measurements and used in an *ad hoc* configuration. The entrance pupil of the telescope is illuminated with a scanning collimated beam which orientation wrt to the telescope entrance pupil can be changed. Scans of the field of view in both directions (denoted by theta in Figure 6) were performed for different orientations of the telescope around its axis (denoted by beta in Figure 6) . The signal at the telescope focal plane is integrated on a matrix of detectors located in the focal plane. Thus for a given field point, after completion of the pupil scanning, the signal integrated over all the detectors provides a measurement of the NDI.

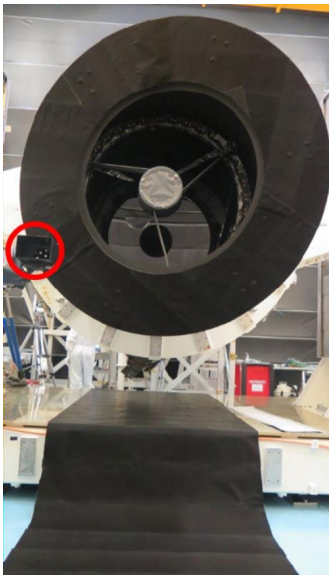

Figure 5. Front view of the telescope in the NDI measurement configuration. *Courtesy of Airbus Defense&Space.*

In Figure 6 are shown only the maximum NDIs derived from the measurements. Minor deviations were found for small angles but are deemed negligible with no impact on the scientific performance.

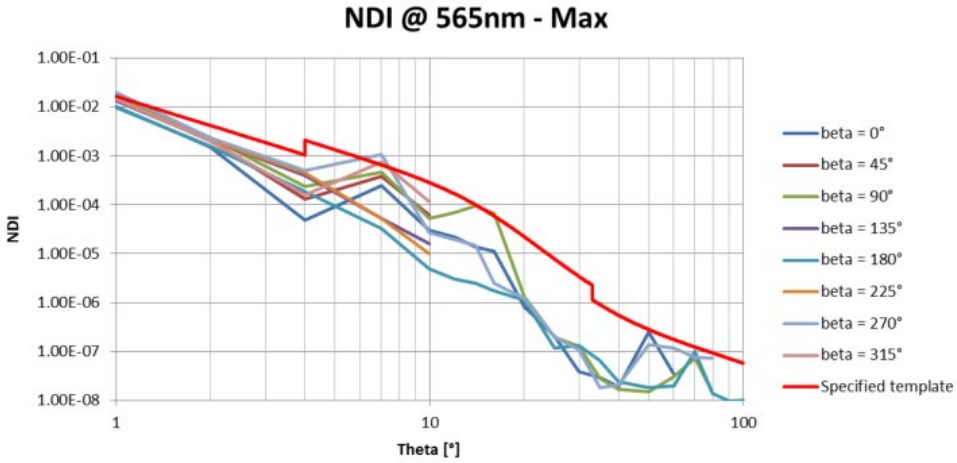

Figure 6. NDI derived from the signal measured on the detectors matrix in the telescope focal plane. *Courtesy of Airbus Defense&Space.*

2.4 Quilting

The primary mirror of the telescope will induce a level of some quilting which could have an impact on the knowledge on the Point Spread Function (PSF) shape which is of utmost importance for the Euclid mission. The relative level of contribution due to quilting was derived from an image of the a monochromatic PSF and by determining the relative level

of the quilting diffraction peaks signal with respect to the core of the PSF, see Figure 7. This way a ratio of 10^{-6} was found, which is about the same order than the tolerated ghosts levels. The quilting though is deterministic and can be predicted.

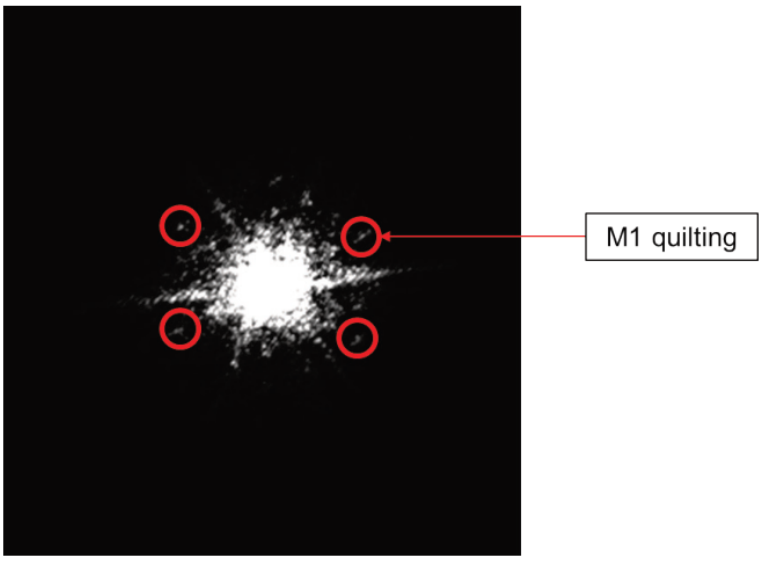

Figure 7. PSF acquired during the M1 quilting characterization. *Courtesy of Airbus Defense&Space.*

3. TESTS IN THERMAL VACUUM CONDITIONS

The test campaign was utterly complex to define design and implement within the practical constraints. More than 60 different tests were carried out in order to fully validate and characterize the performance and functional aspects of the payload. The tests addressing performances were the core of the campaign. Due to lack of space it is not possible here to include all the tests and their results. In the current paper we will focus on the main tests only demonstrating the overall stability end to end of both the payload alignment and optical performance. The tests required a collimated light source to mimic a star (point source) at the telescope entrance pupil. This is achieved using a dedicated collimator (shown in Figure 8) developed by the company AMOS (Belgium).

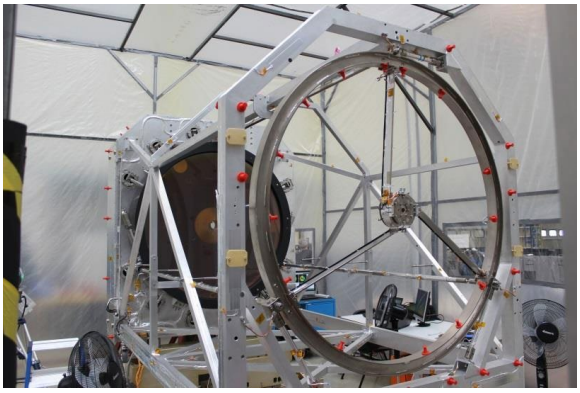

Figure 8. Front view of the collimator.

3.1 Instruments relative alignment and defocus

To obtain a proper sky coverage by both instruments, the overlap of the field of views must be known. In addition, the detectors of both instruments must be in their respective best focus position at the same time. This characterisation was to ensure that under operational conditions, the best focus is achieved simultaneously for both instruments over the entire detector planes.

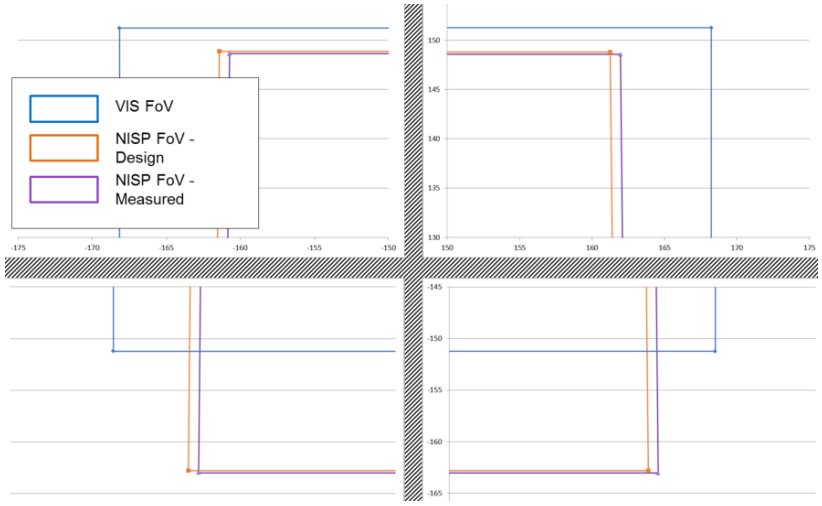

Figure 9. Instruments field of view relative overlap determined from the measurements done during the tests. Units are in millimeters. The VIS field of view is used as the reference. *Courtesy of Airbus Defense&Space.*

The field of view measurements presented in Figure 9 show that the field overlap in 2 dimensions is ensured. However a relative tip/tilt of the fields will induce a relative defocus. Images taken with the detector assembly of the VIS instrument were used to search for across both field of views. The measurements performed had showed that at most the relative defocus amounts to at most -166µm in the telescope focal plane; this value is, to be compared within the allocation of ±400µm.

3.2 Image quality metrics

To complement the previous tests, the image quality metrics of the PSF for both instruments were derived and compared to the predictions including taking into account the gravity contribution. For the VIS instrument the PSF is quantified with the metrics shape[9] R^2 and ellipticity ϵ, for the NISP instrument the encircled energies EE50 at 50% and EE80 at 80% are used.

For the VIS instrument, 25 PSFs for positions around 5 field points were acquired. The metrics for each of them were derived. It was then found that while the metric ϵ is well within the allocation, the metric R^2 exceeds the allocation after correction of the collimator contribution (see Figure 10). This excess was found to be due to a lack of knowledge of the contribution of the detector to the PSF shape, pointing to a need for further calibrations in-flight.

For the NISP instrument, the same strategy was used, with different metrics. Three different laser diodes were used, one per photometric band of the instrument. In that case we found no discrepancies with the predictions were found and the values for the encircled energies EE50 and EE80 were found well within the allocated values. This result combined with the results of the previous section demonstrated the stability and the excellent behaviour end to end of the payload under operational temperature.

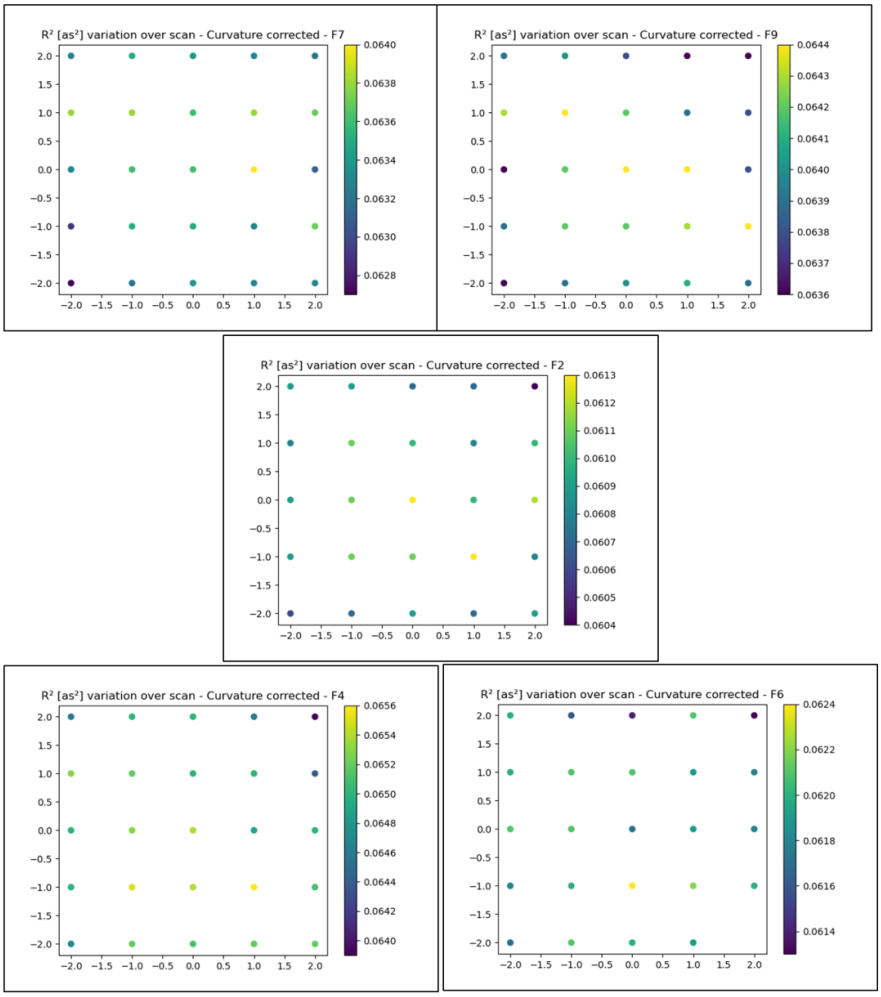

Figure 10. Distribution of the metric R^2 around 5×5 field points of the VIS field of view. The axis are the coordinates in millimetres from the field point considered. *Courtesy of Airbus Defense&Space.*

3.3 Ghost ratio

The masking by image processing of optical ghosts generated by the telescope is important for the success of the Euclid mission. Such removal is efficient only if the ghosts have a negligible levels compared to the core of the PSF. To characterize it, a halogen light source is used with the collimator during the measurements. The ghost generated by the dichroic back surface is clearly visible in Figure 11. The test allocation was computed from the spectral reflectance/transmittance measurements of the different optical elements in the telescope and the spectrum of the halogen light source. The measured the ghost ratio derived is 3.4e-7, to be compared to the test allocation prediction of 7.6e-7.

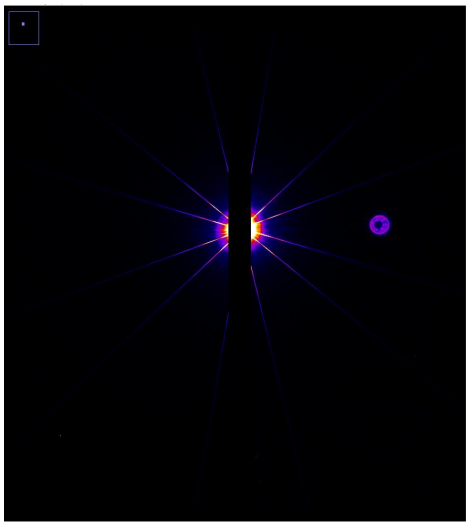

Figure 11. Image acquired by the VIS detector. The dichroic ghost is clearly visible on the right. *Courtesy of Airbus Defense&Space.*

3.4 Thermal settling

The stability of the overall optical path was checked by executing 2 thermal cycles between ambient (20°C) and operational (about 120 K for VIS and about 90 K for NISP) temperatures. The best focus search was performed by actuating the M2 mechanism once the temperature of the payload was stabilised. The values for the M2 position were then compared with the ones achieved in the same temperature conditions. During the cool-down phases and warm-up, images acquisition wase done and the focus was corrected with the collimator by moving the fibre tip at the collimator focal plane . The derived equivalent M2 actuation followed accurately the predictions (see Figure 12). It was identified that the telescope defocus is mostly driven by the deformation of the telescope's primary mirror.

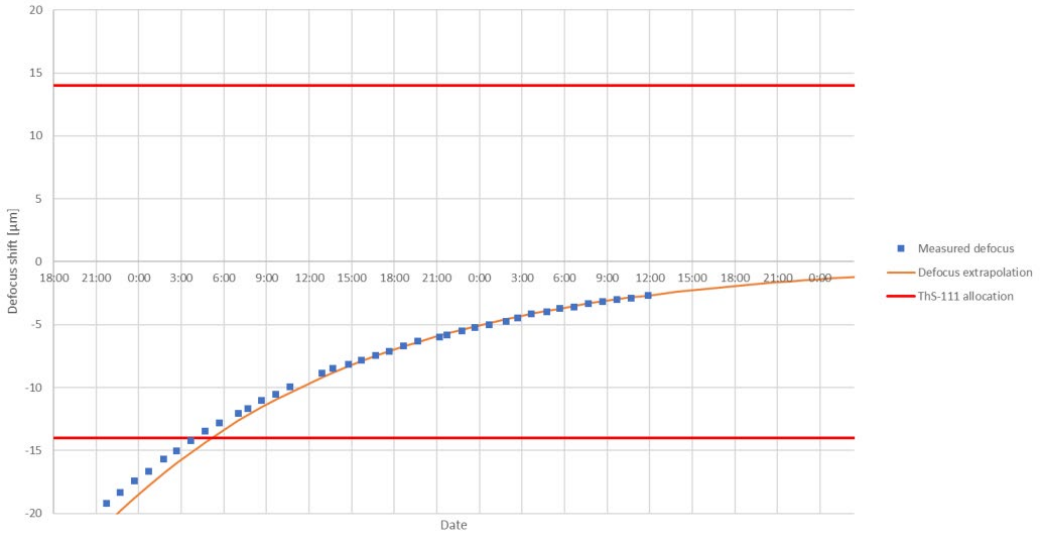

Figure 12. Temporal evolution of the telescope defocus. *Courtesy of Airbus Defense&Space.*

A first thermal cycle evidenced a settling in the best focus position at ambient position. A second cycle was performed and the best focus position for the M2 at operational temperature for each cycles was determined and the obtained values compared with the position of the first cycle. The achieved value is commensurate,, within the focus search accuracy, with both the defocus predicted by thermos-mechanical modelling and the defocus determined with the collimator thus demonstrating the predictability and stability of the defocus behaviour of the payload with the temperature.

4. CONCLUSIONS

After a successful test campaign at ambient of the telescope alone, the qualified instruments were integrated in the Euclid payload module. The end-to-end characterisations and testing of the performances were successful and demonstrated that the entire integrated payload behaviour can be accurately predicted and is behaves as predicted and within the requirements. It is worth noting that the excellent stability of the imaging capabilities can be attributed to the consistent use of silicon carbide for both the telescope and the instruments. A considerable amount of data was gathered during this campaign and will be used further for the assessment of the in-orbit payload performances during the first months after the launch and during the mission.

REFERENCES

[1] ESA, "Euclid Mapping the geometry of the dark universe", ESA/SRE(2011)12, July 2011, http://sci.esa.int/euclid/48983-euclid-definition-study-report-esa-sre-2011-12/#.

[2] Cropper, M., Hoekstra, H., Kitching, T., Massey, R., Amiaux, J., Miller, L., Mellier, Y., Rhodes, J., Rowe, B., Pires, S., Saxton, C. and Scaramella, R., "Defining a weak lensing experiment in space," Monthly Notices of the Royal Astronomical Society 431(4), 3103–3126 (2013).

[3] Racca, G. D., Laureijs, R., Stagnaro, L., Salvignol, J.-C., Alvarez, J. L., Criado, G. S., Venancio, L. G., Short, A., Strada, P., Bönke, T., Colombo, C., Calvi, A., Maiorano, E., Piersanti, O., Prezelus, S., Rosato, P., Pinel, J., Rozemeijer, H., Lesna, V., et al., "The Euclid mission design," Space Telescopes and Instrumentation 2016: Optical, Infrared, and Millimeter Wave 9904, 99040O, International Society for Optics and Photonics (2016).

[4] Cropper, M., Pottinger, S., Azzollini, R., Szafraniec, M., Awan, S., Mellier, Y., Berthé, M., Martignac, J., Cara, C., Giorgio, A.-M. D., Sciortino, A., Bozzo, E., Genolet, L., Philippon, A., Hailey, M., Hunt, T., Swindells, I., Holland, A., Gow, J., et al., "VIS: the visible imager for Euclid," Space Telescopes and Instrumentation 2018: Optical, Infrared, and Millimeter Wave 10698, 1069828, International Society for Optics and Photonics (2018).

[5] Maciaszek, T., Ealet, A., Jahnke, K., Prieto, E., Barbier, R., Mellier, Y., Beaumont, F., Bon, W., Bonnefoi, A., Carle, M., Caillat, A., Costille, A., Dormoy, D., Ducret, F., Fabron, C., Febvre, A., Foulon, B., Garcia, J., Gimenez, J.-L., et al., "Euclid Near Infrared Spectrometer and Photometer instrument concept and first test results obtained for different breadboards models at the end of phase C," Space Telescopes and Instrumentation 2016: Optical, Infrared, and Millimeter Wave 9904, 99040T, International Society for Optics and Photonics (2016).

[6] F. Grupp, E. Prieto, N. Geis, A. Bode, R. Katterloher, R. Grange, V. Junk, and R. Bender, "The optical baseline concept of the NISP near infrared spectrometer and photometer on board of the ESA/EUCLID satellite", Proc. SPIE 8442, p. 84420X–84420X–11 (2012)

[7] Luis M. Gaspar Venancio, Lionel Carminati, Jérôme Amiaux, Luciana Bonino, Giuseppe Racca, Roland Vavrek, René Laureijs, Alex Short, Tobias Boenke, Paolo Strada, "Status of the performance of the Euclid spacecraft," Proc. SPIE 11443, Space Telescopes and Instrumentation 2020: Optical, Infrared, and Millimeter Wave, 114430G (15 December 2020); https://doi.org/10.1117/12.2562490

[8] Pierre Y. Bely, [The design and construction of large optical telescopes], Astronomy & Astrophysics library, Springer Verlag, New-York, p.192 (2003)

[9] Venancio, L. M. G., Laureijs, R., Lorenzo, J., Salvignol, J. C., Short, A., Strada, P., Vavrek, R., Vaillon, L., Gennaro, C., Amiaux, J. and Prieto, É., "Euclid payload module: telescope characteristics and technical challenges," Space Telescopes and Instrumentation 2014: Optical, Infrared, and Millimeter Wave 9143, 91430I, International Society for Optics and Photonics (2014)